Award Accounts

The Chemical Society of Japan Award for Young Chemists for 2007

Molecular Spectroscopic Imaging Using a White-Light Laser Source

Hideaki Kano[1,2]

[1]Department of Chemistry, School of Science, The University of Tokyo, 7-3-1 Hongo, Bunkyo-ku, Tokyo 113-0033

[2]PRESTO (Precursory Research for Embryonic Science and Technology), Japan Science and Technology Agency, 4-1-8 Honcho, Kawaguchi 332-0012

Received January 5, 2010; E-mail: hkano@chem.s.u-tokyo.ac.jp

Coherent anti-Stokes Raman scattering (CARS) microscopy has become a powerful technique for label-free and noninvasive imaging of chemical and biological systems at the molecular level. However, most CARS studies have focused on a limited molecular species such as lipids, and have provided monochromatic images typically at the C–H stretch bands. In the present study, we have extended the CARS technique from monochromatic imaging (microscopy) to multi-color imaging (microspectroscopy). We employed a multiplex CARS process in order to obtain spectral information of the CARS signal. For the broadband Stokes laser, a white-light laser source is used. The white-light laser is generated by injecting ultrashort laser pulses into a novel photonic crystal fiber (PCF). Owing to an ultrabroadband spectral profile of the white-light laser, a wide range of the vibrational resonances can be investigated. We performed label-free and multi-color molecular spectroscopic imaging of biological samples through the multiplex CARS process.

1. Introduction

Focusing light pulses with high peak power under a microscope, we can achieve high photon density both in temporal and spatial domains. It can be effectively used to generate various nonlinear optical processes under a microscope. Even if the nonlinear optical process is well known, combination with microscopy enables us to explore new aspects of nonlinear optical processes which have not been noticed yet. As a result, various kinds of new and unique imaging methods have been developed so far using nonlinear optical processes.

One of the most well-known, widely used, and successful techniques is two-photon excitation fluorescence microscopy.[1] Webb et al. developed two-photon excitation fluorescence microscopy using a femtosecond laser source, and reported visualization of stained chromosomes inside of a living cell with three-dimensional spatial resolution.[1] Because of the near-infrared (NIR) laser irradiation, two-photon excitation fluorescence microscopy is not severely hampered by photobleaching and/or photo-toxic effects, which is often problematic in the case of one-photon fluorescence microscopy. Moreover, thanks to the large penetration depth of NIR light, we can investigate a deep portion of a tissue sample. Besides two-photon excitation fluorescence microscopy, three-photon[2,3] and four-photon[4] excitation fluorescence microscopy have also been reported.

Even-order nonlinear optical processes such as second harmonic generation (SHG) have also been applied to microscopy. In 1974, Hellwarth et al. reported imaging of ZnSe polycrystal using SHG.[5] SHG microscopy has been employed to visualize collagen, microtubule, and muscle fiber.[6,7] Combined with polarization measurement, orientation of collagen fibers has also been investigated.[8] On the other hand, Silberberg et al. have reported third harmonic generation (THG) microscopy and visualization of neurons[9,10] THG can be generated through optical heterogeneity at a focal area such as an interface where refractive index is sharply changed. Moreover, optical Kerr effect (OKE) has also been applied to evaluate diffusive dynamics of water molecules inside of a cell.[11]

2. CARS Microscopy: Development, Principle, and Its Limitation

Among various nonlinear optical effects and nonlinear optical spectroscopic techniques, nonlinear vibrational spectroscopy is one of the most powerful methods, because it enables us to obtain molecular-level information from a sample using "fingerprint" vibrational spectra under a microscope. In particular, nonlinear Raman spectroscopy is a promising method which is applicable to life, medical, and material sciences, because the signal intensity is not affected by water absorption.

Nonlinear Raman spectroscopy was applied to microscopy for the first time in 1982. Duncan et al. have employed coherent anti-Stokes Raman scattering (CARS), a nonlinear Raman effect, and have reported a CARS image at the O–D stretch mode of an onion skin sample soaked with deuterated water.[12]

Published on the web June 24, 2010; doi:10.1246/bcsj.20100004

They have used synchronized two dye lasers. Thanks to the recent development of state-of-the-art solid-state laser sources, CARS imaging systems have been improved significantly. Using a femtosecond Ti:sapphire amplifier and an optical parametric amplifier (OPA), living cell imaging has been reported by Zumbusch[13] and Hashimoto.[14] The repetition rate of the laser source has been increased by using a direct output from a laser oscillator. Cheng et al. have reported laser scanning CARS microscopy using two outputs from synchronized Ti:sapphire oscillators.[15] Dudovich et al. have developed CARS microscopy using a single Ti:sapphire oscillator combined with a spatial light modulator, by which the pulse envelope is modulated to excite a particular Raman band in the CARS process.[16] A Ti:sapphire oscillator has also been used as the pump laser for a cavity-dumped optical parametric oscillator (OPO). Potma et al. reported development of a CARS microscope using an OPO system with a repetition rate of 800 kHz.[17] More recently, a picosecond mode-locked Nd:YVO_4 oscillator and an OPO system has been used for the light source of a CARS microscope, and it allows performance of in vivo measurement of living tissue at video rate.[18] In addition, theoretical approaches to CARS microscopy have also been explored.[19–22] Since several review articles on CARS microscopy have been published,[23–27] we will briefly describe CARS microscopy, and focus on CARS microspectroscopy.[28]

Figure 1a shows a schematic of the CARS process. In the CARS process, two laser pulses with different angular frequency are used to generate a vibrational coherence. These lasers are called ω_1 and ω_2 lasers, or pump and Stokes lasers. If the angular frequency difference, namely $\omega_1 - \omega_2$, matches a particular molecular vibration, Ω, coherent molecular vibration is excited. The vibrational coherence can be converted to third-order nonlinear polarization by the interaction of the molecules with the third laser pulse, ω_3 laser or probe laser. As a result, a CARS field is generated through the third-order nonlinear polarization. As shown in Figure 1a, the third-order nonlinear polarization is created by the interaction of molecules with the

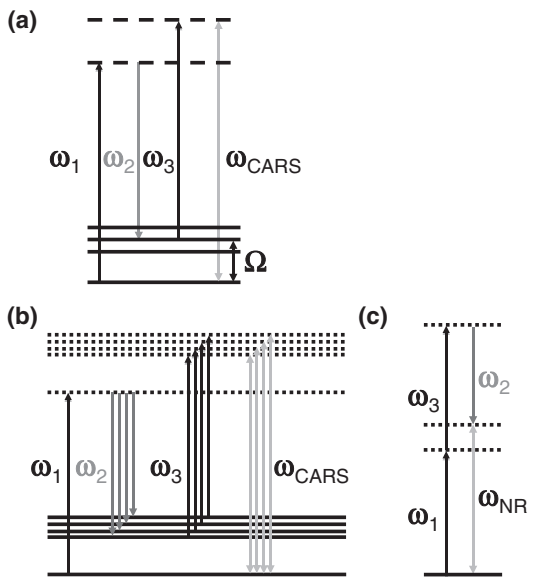

Figure 1. Schematics of CARS (a), multiplex CARS (b), and nonresonant background (c).

ω_1, ω_2, ω_3 (pump, Stokes, and probe) laser pulses. According to energy and momentum conservation laws, the angular frequency and wave vector of the CARS field, ω_{CARS}, $\mathbf{k}_{CARS}$ should satisfy the following equation;

$$\omega_{CARS} = \omega_1 - \omega_2 + \omega_3 \quad (1)$$

$$\mathbf{k}_{CARS} = \mathbf{k}_1 - \mathbf{k}_2 + \mathbf{k}_3 \quad (2)$$

Here $\mathbf{k}_x$ corresponds to the wave vector of ω_x-laser. In order to simplify the experimental setup, the ω_1 laser is often used for the ω_3 laser as well. In this condition ($\omega_3 = \omega_1$ and $\mathbf{k}_1 = \mathbf{k}_3$), the intensity of the CARS signal is quadratically and linearly proportional to the intensity of the ω_1 and ω_2 lasers, respectively. In other words, the CARS signal intensity shows nonlinear dependence on that of the incident laser, ω_1. Concerning the phase-matching condition, or momentum conservation law, the CARS field has a well-defined wave vector. It means that the CARS field propagates unidirectionally. We can therefore detect the signal more efficiently than the conventional spontaneous Raman signal.

Compared with conventional spontaneous Raman scattering microscopy, there are several advantages to CARS microscopy. First, the detected wavelength of a CARS signal is shorter than those of incident lasers (Strictly speaking, the wavelength of the CARS signal is shorter than that of the probe laser, ω_3). It enables us to obtain the Raman signal even in the presence of one-photon fluorescence background in an electronically resonant condition. Second, because CARS is a third-order nonlinear optical process, it has an inherent three-dimensional sectioning capability without the pinhole required by confocal Raman microscopy. Third, owing to an intense, unidirectional CARS signal, it does not require long data-acquisition time in comparison with spontaneous Raman microscopy. Forth, we can independently control the polarization of the pump, Stokes, and probe laser pulses, and the polarization angle of an analyzer for the signal. Therefore, various polarization measurements can be performed. Fifth, the coherent nature of the CARS signal can be extensively used to measure the real and imaginary parts of the CARS field separately by heterodyne detection.[29,30] CARS microscopy breaks the barrier of the so-called diffraction limit due to the third-order nonlinearity by a factor of $\sqrt{3}$.[31] The reported spatial resolution is typically about 280 and 750 nm in the lateral and axial directions, respectively.[15] In order to improve the spatial resolution, a metal tip[32] or optical near-field[33] have been applied to CARS microscopy. As another approach, direct CARS imaging has also been reported by wide-field laser illumination.[34]

CARS microscopy has so far been applied to various samples, and its usefulness and power have been demonstrated. As examples, there are the following reports. The CARS signal due to the CH_2 stretch vibrational mode has a resonance frequency relatively far from those of incidence lasers. It is therefore fairly easy to measure this signal in comparison with the signal at the fingerprint region, where many Raman bands are congested. The Xie group visualized transportation of lipid droplets inside of live cells using the CARS signal due to the CH_2 stretch vibrational mode. They measured mitochondria labeled with fluorescent protein simultaneously, and traced both signals.[35] The group of Cheng and others have reported the CARS imaging of myelin sheath,[36] observation of

endocytosis in live cells,[37] and application of CARS microscopy to drug delivery.[38] Pezacki's group has reported the simultaneous imaging of lipid droplets (CARS) in living cells and the RNA (two-photon excitation fluorescence) of hepatitis C viruses in order to study interactions between a host and viruses.[39] The group of Turner and others has reported screening of embryonic stem cells by CARS microscopy, and performed high speed and nondestructive assays.[40] Moreover, the group of Enejder and others has investigated lipid storage in nematodes (*Caenorhabditis elegans*), models of multicellular organisms.[41] More recently, ex vivo visualization of brain tissue,[42] application to flow cytometry,[43] and visualization of catalysts[44] have been reported by CARS microscopy.

As mentioned above, CARS microscopy has been developing and been applied to many fields. However, it only provides a so-called "black and white" image with a particular Raman band such as CH_2 stretch vibrational mode. The situation is similar to stimulated Raman (Raman gain and/or Raman loss) microscopy, which has been recently reported.[45] In order to utilize effectively the wealth of information in vibrational spectra, it is necessary to obtain not only CARS images but also CARS spectra. It has been a challenge to develop a CARS microspectroscopic system which is capable of obtaining both CARS spectra and images, because the laser wavelength should be tuned for obtaining CARS spectra in a conventional setup.

3. CARS Microspectroscopy

3.1 Multiplex CARS. With the use of a CARS microspectroscopic system, (pseudo-)multi-color images can be obtained by evaluating multiple vibrational resonances in CARS spectra. Although several methods might be used to obtain CARS spectra, one well-established method is a multiplex CARS process described in the following. The outline of multiplex CARS is shown in Figure 1b. In multiplex CARS, two laser sources with narrow-band and broad-band spectral profiles are used for the pump (ω_1) and Stokes (ω_2), respectively. Therefore, a wide distribution arises in the angular frequency difference, $\omega_1 - \omega_2$. Consequently, multiple combinations of $\omega_1 - \omega_2$ take place to match the vibrational resonances of sample molecules. In this way, multiple vibrational coherences are generated. Subsequently, these coherences are probed by the third laser pulse or probe laser (ω_3), giving rise to a CARS signal with various angular frequencies of $\omega_1 - \omega_2 + \omega_3$. Using a spectrometer, the CARS signal is spectrally dispersed, and the CARS spectrum is finally detected with multiple sharp features due to vibrational resonances. A typical CARS spectrum is shown in Figure 2.[46] The sample is a polystyrene bead and the spectral profile of the CARS signal has been intensity-corrected (vide infra). As depicted in Figure 2, the spectral profile shows a dispersive lineshape. This is due to an interference effect of the CARS signal with the so-called nonresonant background (NBG). As is the case of CARS, NBG is a third-order nonlinear optical process, in which no vibrational resonance contributes to the optical process. One schematic for NBG is shown in Figure 1c. Although NBG is "nonresonant" for a vibrational transition, the intensity is increased if the value of $\omega_1 + \omega_3$ approaches the electronic transition energy (Figure 1c). If the value of $\omega_1 + \omega_3$ is far from an electronic resonance, namely, if the sample is transparent, the NBG should give a flat spectral profile. In reality however, the spectral profile of the NRB is distorted mainly by that of the Stokes laser, diffraction efficiency of the polychromator, and wavelength-dependent sensitivity of the CCD camera. It is also true for the spectral profile of the vibrationally resonant CARS signal. Since this distortion is the same for CARS and NBG, we can correct the intensity of the CARS signal using NBG. The procedure of the intensity correction is in the following. First, NBG is measured with the same experimental setup as the sample in order to avoid any additional distortion of the spectral profile. Second, the CARS signal intensity is divided by that of NBG at each spectral component. In the present study, NBG of a cover glass is used, because it can be obtained by minimum adjustment of the setup, namely just by changing the axial position of the sample. The intensity-corrected CARS spectrum (Figure 2) shows simultaneous measurement of the CARS signal with a broad area from the fingerprint region to the C–H stretch region. The spectral coverage is $>3500\,cm^{-1}$, which means that most of the fundamental modes of a molecule can be detected. Such ultrabroadband spectral coverage for multiplex CARS was difficult to realize using a conventional laser source.[47–50] The supercontinuum,[51] or white-light laser source, which is generated with a photonic crystal fiber,[52–54] has enabled us to perform ultrabroadband multiplex CARS.

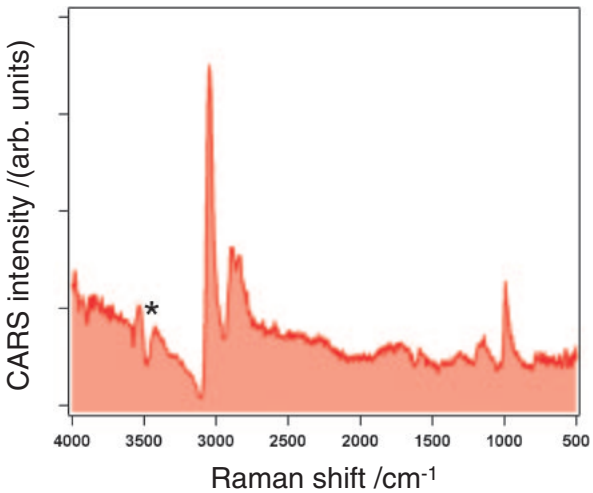

Figure 2. Intensity-corrected CARS spectrum of a polystyrene bead with a diameter of 10 μm (adapted from Ref. 46 with permission). A sharp structure at $3500\,cm^{-1}$ indicating as "*" is an artifact due to the intensity correction.

3.2 Photonic Crystal Fibers. Photonic crystal fiber (PCF) is a fiber which has periodic microstructures in the cladding region.[52–54] After the first PCF was reported in 1996,[53] the fabrication procedure has been improved remarkably for fine control of various optical properties such as dispersion, birefringence, and nonlineality. In particular, the PCF for genarating white-light laser radiation (supercontinuum) consists of a core with a small diameter (the core diameter in the present study was 1.7 μm) and a surrounding cladding region with many air holes arranged like a honeycomb structure. The laser pulses introduced into the PCF are tightly confined in the

small core due to the large refractive index difference between core (silica) and cladding with air holes. Moreover, dispersion properties of the PCF can be controlled by tuning the size of air holes and their arrangement. As the result of strong confinement of the optical field and fine adjustment of the dispersion properties of PCFs, ultrashort laser pulses with broad spectral bandwidth propagate through a PCF without sufferring temporal broadening due to group velocity dispersion. Since the photon density can be kept at a high level temporally and spatially inside of the PCF, various nonlinear optical effects take place through the propagation. Supercontinuum, or white-light laser, is generated as a result of such series of nonlinear optical effects. Thanks to PCFs, the peak power to generate supercontinuum is drastically decreased from MW to kW. Therefore, the direct output from a femtosecond laser oscillator can be seeded into a PCF to generate supercontinuum or white-light laser. It means that we do not need any complicated laser system such as laser amplifiers or cavity dumpers. The spectral bandwidth of white-light laser has been drastically extending further and further. The generation of white-light laser radiation from 350 to 3000 nm[55] and that from 789 to 4870 nm[56] have been reported by injecting femtosecond laser pulses at 1550 nm. Moreover, white-light laser can also be generated even with nanosecond laser pulses,[57,58] and the laser sources are getting smaller and smaller.

Application of white-light laser sources to microscopes has been reported since around 2003, and various types of unique microscopes have been developed so far such as confocal fluorescence microscopes,[59–62] two-photon excitation fluorescence microscopes,[63,64] fluorescence lifetime microscopes,[65,66] CARS microscopes[28,67–71] and a STED (stimulated emission depletion) microscope.[72] There is also a report on optical tweezers using a white-light laser source.[73] In addition, efficient generation of a multi-photon process has been reported by controlling the amplitude and phase of white-light laser pulses.[74]

3.3 Development of a Multiplex CARS Microspectroscopic System. Figure 3 shows a schematic of the ultrabroadband multiplex CARS microspectroscopic system developed by us.[28,75,76] The laser source is a mode-locked Ti:sapphire laser oscillator (Vitesse, Coherent Inc.). A portion of the output was seeded into the PCF (NL-PM-750, Crystal Fiber Inc.) in order to generate white-light laser. The spectral profile of the white-light laser ranges from visible to NIR. In the present study, only the NIR spectral components were selected for a broadband Stokes laser (ω_2). The remaining fundamental from the oscillator was spectrally filtered by a custom-made narrow band-pass filter, and was used for the pump laser (ω_1). The spectral bandwidth of the pump laser is about 20 cm^{-1}. The two laser pulses, namely the pump and Stokes pulses, were superposed collinearly with a notch filter after adjusting the temporal timing between them with a delay stage. The two co-propagating laser pulses were introduced into an inverted microscope (TE-2000, Nikon), and were tightly focused onto the sample by a microscope objective lens. Although the phase-matching condition should be satisfied for the CARS process, it is relaxed by the high NA value (0.9 for the present setup) of the microscope objective lens. As a result, the CARS signal is generated in a broad wavenumber region so as to be covered with all fundamental vibrational modes. The CARS signal was collected by another microscope objective lens which is placed facing the first one. After passing through a couple of optical filters, the signal is dispersed by a polychromator (SpectraPro 300, Acton Inc.), and is detected by a CCD camera (Spec-10:400BR/XT or PIXIS 100B, Roper Scientific Inc.). In order to reduce the read-out time for each spectrum, only a portion of the CCD area was used for the detection of the CARS signal. Samples were placed on a 3-axial piezo stage (Nano-LP-100 or Nano-LP-200, Mad City Labs). The samples were scanned at a particular spatial region of interest with measurement of CARS spectra at each position. Finally, CARS images were reconstructed using the multiple vibrational resonances.

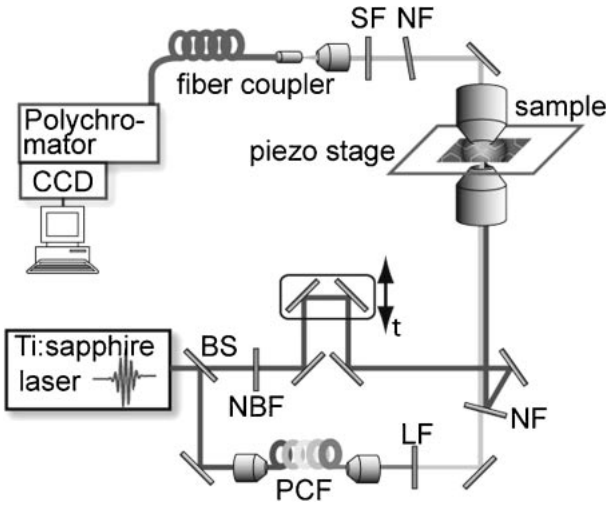

Figure 3. Experimental setup for multiplex CARS microspectroscopy: BS: beam splitter, NBF: narrow band-pass filter, LF: long-wavelength pass filter, NF: Notch filter, SF: short-wavelength pass filter.

Since CARS is a third-order nonlinear optical process, signal is generated only at the position where the laser pulses are tightly focused. Consequently, three-dimensional spatial resolution can be realized without using a confocal pinhole. The spatial resolution in the present study is about 0.5 and 1.5 μm in the lateral and axial directions, respectively.[77]

3.4 Spectral Analysis of Multiplex CARS Spectra. As shown in the previous subsection, we can obtain multiple sharp features due to vibrational resonances in the CARS spectrum. In fact, CARS spectroscopic imaging provides not only such CARS spectra but also a unique analytical method to extract only a vibrationally resonant signal from the spectra. As described in Section **3.1**, the CARS spectrum is a superposition of the vibrationally resonant and nonresonant signals. Therefore, if an image is constructed just using the signal intensity, it gives an image originating not only from the vibrationally resonant signal but also NBG. Therefore, NBG is often regarded as "contamination," and great efforts have been made to eliminate NBG. We, however, make use of NBG in order to efficiently extract vibrationally resonant components from the "contaminated" CARS spectrum.[69] The method is based on the unique characteristic that both CARS and NBG are coherent with each other.[78] The procedure is described in the following.

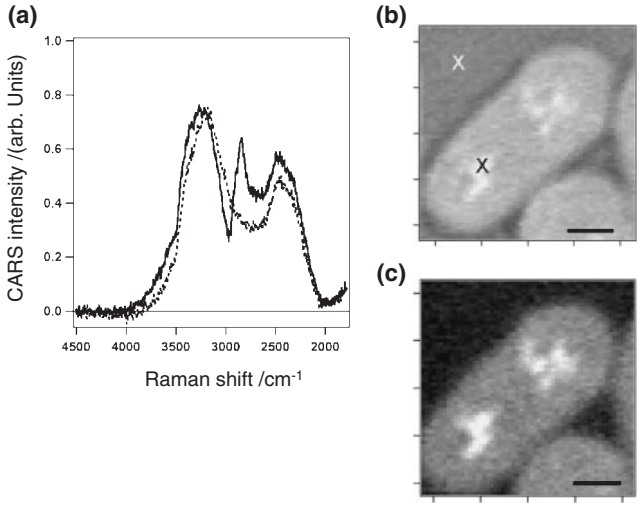

Figure 4. (a) Typical spectral profile of the CARS signal of a living yeast cell (solid) and surrounding water (dotted) and (b) CARS image of living yeast cells at the Raman shift of 2856 cm^{-1}, vibrationally resonant CARS image at the CH stretch vibrational mode. The short bar measures 2 μm. CARS spectra (solid and dotted) in (a) are obtained at the black and white crosses in (b), respectively; (c) CARS image after the spectral analysis.

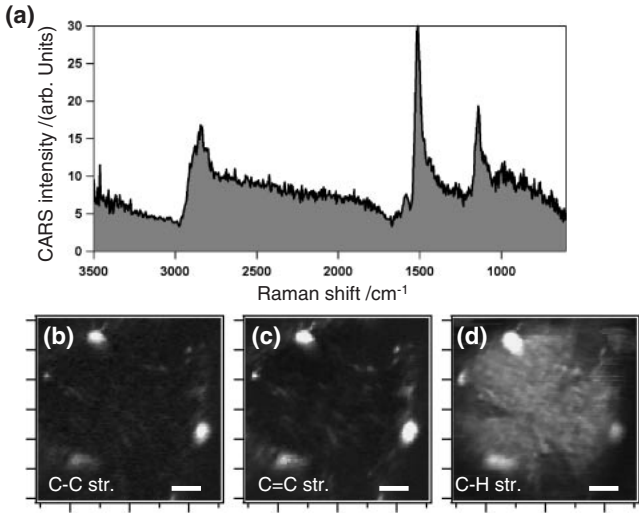

Figure 5. (a) CARS spectrum (intensity corrected) of a single pollen grain; CARS images of a pollen grain at C–C (b), C=C (c), and C–H (d) stretch vibrational mode. The short bar measures 5 μm.

The signal obtained with the CARS microspectroscopic system is described in the following formula in general;

$$I(\omega) = \left| A_{\mathrm{NR}} e^{i\phi} + \sum_{\mathrm{R}} \frac{A_{\mathrm{R}}\Gamma_{\mathrm{R}}}{\Gamma_{\mathrm{R}} - i(\omega - \Omega_{\mathrm{R}})} \right|^2 \quad (3)$$

Here $I(\omega)$ is the overall signal intensity, A_{NR} and ϕ are the amplitude and the phase of NBG, A_{R} is the amplitude of the CARS signal, Ω_{R} is the angular frequency of the vibrational resonance, and Γ_{R} is a factor proportional to the linewidth. For simplicity, we assume that no electronic state is resonant with the incident optical field. As discussed, the NBG (first term) and the vibrationally resonant CARS signal (second term) interfere with each other, and the spectral profile becomes dispersive. In other words, the spectral profile at a particular CARS resonance gives a dip and peak at high and low wavenumber, respectively. It means that the CARS signal is heterodyne-detected with the use of NBG. Based on such a meaningful spectral pattern and eq 3, we can extract only a vibrationally resonant CARS signal. As an example, Figure 4a shows a typical spectral profile of the CARS signal (solid) with NBG interference. The sample is a fission yeast cell. Figure 4a also shows NBG due to water (dotted). Figure 4b shows the intensity mapping of the CARS signal at 2856 cm^{-1}. Owing to the non-negligible intensity of NBG, the contrast is significantly degraded. On the other hand, if we perform the spectral analysis described above, the contrast originates purely from vibrational resonance, namely A_{R}. The resultant image is shown in Figure 4c. It is clear that the contrast is significantly improved. It is noted that the spectral analysis does not depend on whether NBG comes from intracellular molecules or water, because both NBG give approximately the same spectra due to absence of any electronic resonance. In other words, the vibrationally resonant component can be extracted quantitatively using eq 3, if we can assume that NBG give the same spectral profile at the measured area. CARS microspectroscopy thus provides improvement of the contrast through spectral analysis, which is not applicable to conventional CARS microscopy. Recently, a novel algorithm using maximum entropy has also been applied to spectral analysis of a CARS signal with a congested spectral profile.[79]

4. Molecular Spectroscopic Imaging

4.1 Single Pollen Grain. Figure 5 shows CARS spectroscopic imaging of a single pollen grain of a cherry blossom.[80] The exposure time is 100 ms. Since pollen emits very strong auto-fluorescence, it is difficult to measure spontaneous Raman spectra. For this reason, pre-treatment such as photo-bleaching by laser irradiation[81] or application of surface-enhanced Raman scattering (SERS)[82] have been reported so far. On the other hand, CARS does not suffer from auto-fluorescence, because the signal wavelength is blue shifted from those of the incident lasers. As a result, we have successfully obtained the CARS spectrum of a single pollen grain without any pretreatment. The multiplex CARS spectrum (intensity corrected) shown in Figure 5a consists of several peaks due to vibrational resonances. In particular, three peaks at around 1150, 1520, and 2850 cm^{-1} are prominent. Figures 5b–5d show the CARS images at around 1150, 1520, and 2850 cm^{-1}, respectively. It is clear that Figures 5b and 5c show the same image, indicating that these vibrational modes originate from the same molecular species. On the other hand, Figure 5d shows a different image from Figures 5b and 5c, giving the whole shape of the pollen grain. Taking into account that the spectral profile in the fingerprint region is similar to that of β-carotene,[80] the bands at around 1150 and 1520 cm^{-1} are ascribed to C–C and C=C stretch vibrational modes due to carotenoid derivertives. On the other hand, the band at around 2850 cm^{-1} is attributable to C–H stretch vibrational modes of long alkyl chains contained in lipid molecules. Interestingly, spatial overlap is found at the

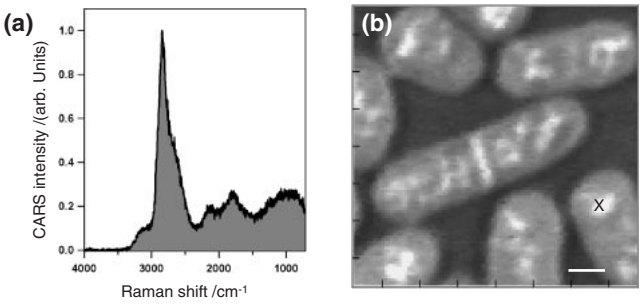

Figure 6. (a) Typical spectral profile of the CARS signal from a living yeast cell and (b) CARS image of living yeast cells at the Raman shift of CH stretch vibrational mode. The short bar measures 2 μm. The CARS spectrum (a) is obtained at the black cross in (b).

granular parts in Figures 5b–5d. It means that both carotenoid derivatives and lipid coexist in high concentration in these granular parts. Molecular spectroscopic imaging based on CARS microspectroscopy thus distinguishes each molecular species by spectral information.

4.2 Living Yeast Cell. Figure 6a shows typical spectral profiles of the multiplex CARS signal of a living fission yeast cell (*Schizosaccharomyces pombe*; *S. pombe*).[71] The exposure time was 100 ms. As clearly shown, an intense signal is observed at around the Raman shift of 2850 cm^{-1}. This band originates from the CH stretch vibrational mode, mainly found at membranous organelles such as mitochondria. Figure 6b shows a CARS image at this band. It indicates various yeast cells at different stages of the cell division cycle. In particular, a septum is also visualized inside of the yeast cell around the center of Figure 6b. The septum is composed of polysaccharide, and is also rich in CH bonds.

So far, we have focused on CARS spectroscopic imaging using a white-light laser source. Since it has high peak power, we can observe not only CARS but also multi-photon excitation fluorescence. Figure 7 shows multi-modal nonlinear optical imaging. The sample is a living yeast cell, whose nuclei are tagged by green fluorescent protein (GFP). Simultaneous irradiation of the pump and Stokes laser pulses excites GFP through two-photon excitation. A broad band is found at 520 nm in Figure 7a. It is due to the two-photon excitation fluorescence of GFP. It should be noted that the fluorescence signal is spectrally separated from the CARS signal ranging from 630 to 750 nm. It is therefore easy to perform multi-modal imaging using different spectral components. Figures 7b and 7c show images of the CARS at CH stretch vibrational mode and two-photon excitation fluorescence, respectively.

Since both CARS and two-photon excitation fluorescence are nonlinear optical processes, they have inherent three-dimensional sectioning capability. Figure 8 shows the optical sectioning of a living yeast cell. Both CARS at CH stretch vibrational mode and two-photon excitation fluorescence are shown in (a) and (b), respectively. Each lateral (XY) image was obtained by $\Delta Z = 305$ nm step. In total, 21 images are displayed from the top (upper left) to the bottom (lower right) part of the yeast cell. Exposure time at each spatial point is 50 ms. Based on the three-dimensional vibrational and fluorescence information, the yeast cell can be reconstructed

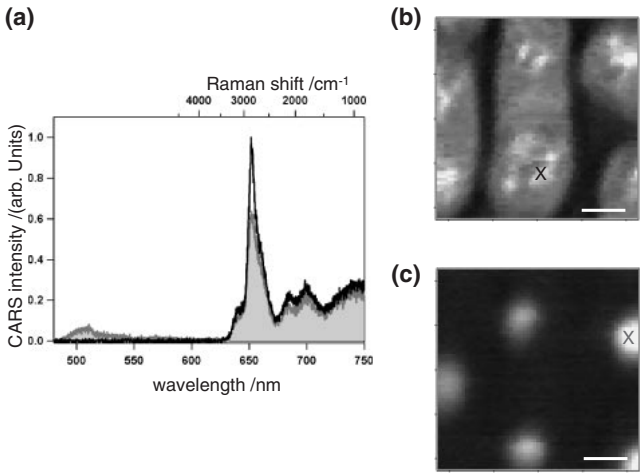

Figure 7. (a) Spectral profile of the CARS and two-photon excitation fluorescence signals of a living yeast cell, (b) CARS image of living yeast cells at the CH stretch vibrational mode, and (c) two-photon excitation fluorescence image of the same system at 506 nm. The black and gray spectra in (a) are obtained at the black crosses in (b) and (c), respectively.

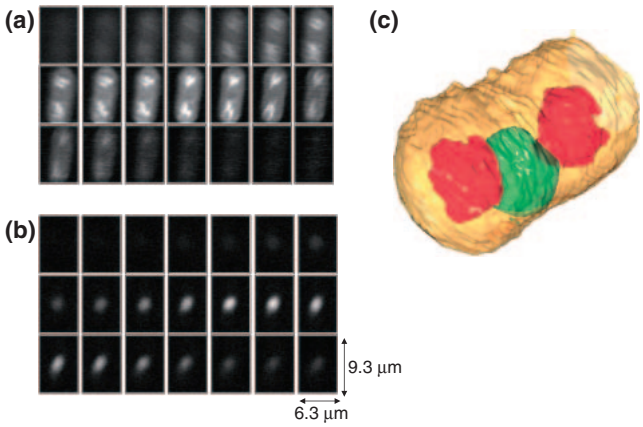

Figure 8. (a) XYZ image stack of the CARS signal at the Raman shift of the CH stretch vibrational mode and (b) XYZ image stack of the two-photon excitation fluorescence signal. The sample is a living yeast cell, whose nucleus is labeled by GFP. Each lateral (XY) image was obtained by $\Delta Z = 305$ nm step. In total, 21 images are displayed from the top (upper left) to the bottom (lower right) part of the yeast cell. Exposure time at each spatial point is 50 ms: (c) Three-dimensional volume rendering of data sets of the CARS and two-photon excitation fluorescence signals. Orange, brown, and green areas correspond to the strong and moderate (about one-half in the intensity in comparison with the orange area) CARS signal intensity, and two-photon excitation fluorescence signal intensity, respectively (adapted from Ref. 46 with permission).

three-dimensionally (Figure 8c). Membranous organelles (red, color on line) and nucleus (green, color on line) are clearly visualized.

Taking advantage of CARS, we can pursue the dynamic behavior of a living cell. Figure 9 shows the in vivo monitoring

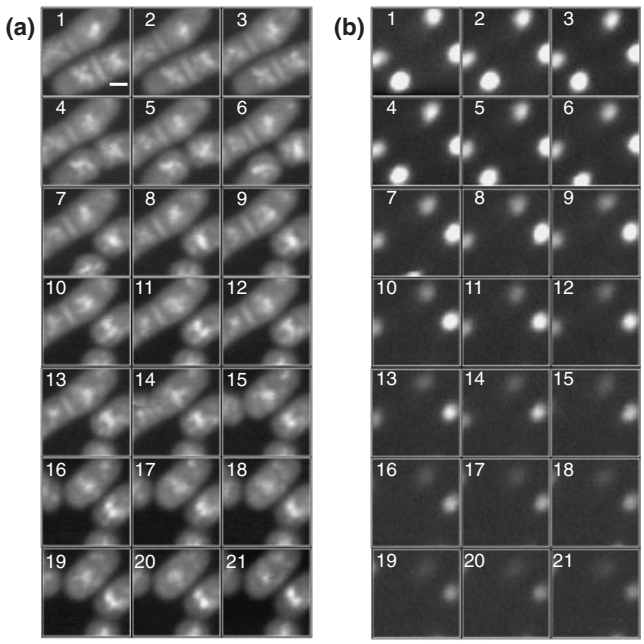

Figure 9. CARS at the CH stretch vibrational mode (a) and two-photon excitation fluorescence (b) images, respectively. The sample is a living yeast cell, whose nucleus is labeled by GFP. The scale bar corresponds to 2 μm. The number at the upper left shows the time course of the observation. Exposure time at each spatial point is 50 ms. Lateral (XY) images consist of 61 × 61 pixels, and are measured in 3.8 min per image (adapted from Ref. 46 with permission).

of a living cell during cell division. Figures 9a and 9b show CARS of the CH stretch vibrational mode and two-photon excitation fluorescence images, respectively. The sample is a living yeast cell whose nucleus is labeled with GFP. The number at the upper left shows the time of observation. Exposure time at each spatial point is 50 ms. Each image consists of 61 × 61 pixels, and is measured 3.8 min per image. The cell division is clearly visualized. It is noted that the signal intensity shown in Figure 9b becomes weaker and weaker in the course of the cell division. It is probably due to photo-bleaching by the laser irradiation. On the other hand, the CARS signal intensity does not deteriorate. This manifests another advantage of CARS imaging, which does not suffer inherently from photo-bleaching.

4.3 Nematodes. The nematode, *Caenorhabditis elegans* (*C. elegans*) is known as a biological model of a multi-cellular organism. It is used for various studies such as generation, behavior, aging, and intracellular signal transmission. In the present study, we have applied our molecular spectroscopic imaging technique to visualize nematodes at the molecular level. The sample is a mutant called unc-119, which shows slow movement in comparison with native organisms. Before measurement, we exposed the sample specimens to a drug called levamisole in order to suppress movement. Figure 10 shows molecular spectroscopic imaging of the CH stretch vibrational mode of a tail region (a) and an abdominal region (b) of a nematode, respectively. Exposure time at each spatial point is 50 ms. It shows various organs inside of the nematode.

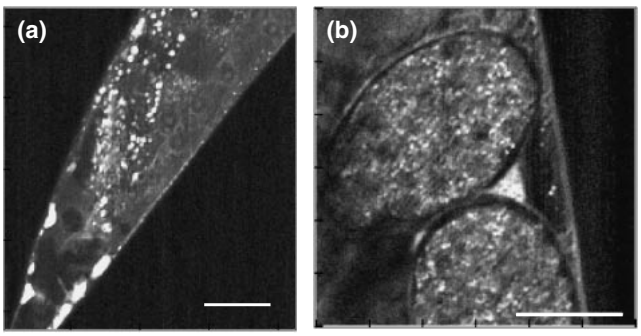

Figure 10. CARS images at the CH stretch vibrational mode of a tail region (a) and an abdominal region (b) of a nematode. Exposure time at each spatial point is 50 ms. The short bar measures 20 μm.

In particular, many small and bright spots are distributed inside of the body in Figure 10a. Taking account that the nematode stores lipid as lipid droplets, these structures are assigned to lipid droplets. At the right part of the body, some cells are aligned with the body line. It is probably a genital gland. On the other hand, large and round organs are observed in Figure 10b. They are eggs. It should be noted that several dark spots are observed inside of the eggs. They are probably nuclei, showing that the eggs contain multiple cells.

5. Concluding Remarks

Owing to its inherent molecular specificity, CARS microspectroscopy is one of the most promising techniques for molecular spectroscopic imaging, since it provides multi-color images with rich spectral information on molecular composition and structure. In comparison with conventional fluorescence imaging, which can visualize only known molecules, CARS spectroscopic imaging can provide information on as-yet-unrecognized molecules through spectral analysis. As a result, CARS spectroscopic imaging enables us to explore such "hidden" molecules and their structures. Development and applications of CARS spectroscopic imaging are currently ongoing. For instance, there are reports on water molecules in lipid bilayer,[83] blend polymer,[68,84] coherence length of a Frenkel exciton in molecular J-aggregates,[77] and high-speed detection of bacteria.[85] From the technological point of view, a new light source, namely sub-nanosecond microchip laser has been built into a CARS spectroscopic system. Since the light source is compact and robust, the overall system is significantly simplified.[86,87]

Combined analysis of CARS with other nonlinear optical processes such as SHG, THG, and two-photon excitation fluorescence enables us to perform unique multi-modal nonlinear optical imaging to gain deep insight into a living system. Among them, hyper-Raman spectroscopy[88] is a unique nonlinear Raman process, because infrared active vibrational modes can be probed. Combination of CARS and hyper-Raman provides unique high-spatial-resolution vibrational microspectroscopy that is not restricted by the selection rules.

Molecular spectroscopic imaging featuring nonlinear Raman processes will open up a new scope for visualization of living cells and organisms in vivo and in situ, and will be an indispensable tool for medical, life, and material sciences.

I would like to express my sincere gratitude to Professor Hiro-o Hamaguchi for his guidance, support, discussion, and encouragement throughout the present study. I would also like to thank all collaborators in the Hamaguchi laboratory for their dedicated efforts in contributing to this study. This work is supported by a Grant-in-Aid for Creative Science Research (No. 15GS0204) from MEXT. H. Kano gratefully acknowledges financial support by the Precursory Research for Embryonic Science and Technology (PRESTO) program of the Japan Science and Technology Agency (JST), Grant-in-Aid for Scientific Research on Priority Areas "Molecular Science for Supra Functional Systems" [477] from MEXT, and the Global COE Program for "Chemistry Innovation." I would also thank Dr. Y.-S. Huang, Mr. T. Nakatsuka, and Mr. Y. Muramatsu for their help in sample preparation, and Dr. T. Karashima and Prof. M. Yamamoto for providing *S. pombe* strain and *C. elegans*.

References

1 W. Denk, J. H. Strickler, W. W. Webb, *Science* **1990**, *248*, 73.
2 S. Maiti, J. B. Shear, R. M. Williams, W. R. Zipfel, W. W. Webb, *Science* **1997**, *275*, 530.
3 M. Schrader, K. Bahlmann, S. W. Hell, *Optik* **1997**, *104*, 116.
4 H. Matsuda, S. Ito, Y. Nagasawa, T. Asahi, H. Masuhara, S. Kobatake, M. Irie, H. Miyasaka, *J. Photochem. Photobiol., A* **2006**, *183*, 261.
5 R. Hellwarth, P. Christensen, *Opt. Commun.* **1974**, *12*, 318.
6 P. J. Campagnola, M.-D. Wei, A. Lewis, L. M. Loew, *Biophys. J.* **1999**, *77*, 3341.
7 P. J. Campagnola, L. M. Loew, *Nat. Biotechnol.* **2003**, *21*, 1356.
8 T. Yasui, Y. Tohno, T. Araki, *Appl. Opt.* **2004**, *43*, 2861.
9 Y. Barad, H. Eisenberg, M. Horowitz, Y. Silberberg, *Appl. Phys. Lett.* **1997**, *70*, 922.
10 D. Yelin, D. Oron, E. Korkotian, M. Segal, Y. Silberberg, *Appl. Phys. B* **2002**, *74*, s97.
11 E. O. Potma, W. P. de Boeij, D. A. Wiersma, *Biophys. J.* **2001**, *80*, 3019.
12 M. D. Duncan, J. Reintjes, T. J. Manuccia, *Opt. Lett.* **1982**, *7*, 350.
13 A. Zumbusch, G. R. Holtom, X. S. Xie, *Phys. Rev. Lett.* **1999**, *82*, 4142.
14 M. Hashimoto, T. Araki, S. Kawata, *Opt. Lett.* **2000**, *25*, 1768.
15 J.-X. Cheng, Y. K. Jia, G. Zheng, X. S. Xie, *Biophys. J.* **2002**, *83*, 502.
16 N. Dudovich, D. Oron, Y. Silberberg, *Nature* **2002**, *418*, 512.
17 E. O. Potma, W. P. de Boeij, P. J. M. van Haastert, D. A. Wiersma, *Proc. Natl. Acad. Sci. U.S.A.* **2001**, *98*, 1577.
18 C. L. Evans, E. O. Potma, M. Puoris'haag, D. Côté, C. P. Lin, X. S. Xie, *Proc. Natl. Acad. Sci. U.S.A.* **2005**, *102*, 16807.
19 E. O. Potma, W. P. de Boeij, D. A. Wiersma, *J. Opt. Soc. Am. B* **2000**, *17*, 1678.
20 J.-X. Cheng, A. Volkmer, X. S. Xie, *J. Opt. Soc. Am. B* **2002**, *19*, 1363.
21 M. Hashimoto, T. Araki, *J. Opt. Soc. Am. A* **2001**, *18*, 771.
22 M. Hashimoto, *Bunko Kenkyu* **2000**, *40*, 51.
23 A. Volkmer, *J. Phys. D: Appl. Phys.* **2005**, *38*, R59.
24 X. S. Xie, J. Yu, W. Y. Yang, *Science* **2006**, *312*, 228.
25 M. Müller, A. Zumbusch, *ChemPhysChem* **2007**, *8*, 2156.
26 J.-X. Cheng, *Appl. Spectrosc.* **2007**, *61*, 197A.
27 C. L. Evans, X. S. Xie, *Annu. Rev. Anal. Chem.* **2008**, *1*, 883.
28 H. Kano, H. Hamaguchi, *Appl. Phys. Lett.* **2005**, *86*, 121113.
29 D. L. Marks, S. A. Boppart, *Phys. Rev. Lett.* **2004**, *92*, 123905.
30 C. L. Evans, E. O. Potma, X. S. Xie, *Opt. Lett.* **2004**, *29*, 2923.
31 J. Squier, M. Müller, *Rev. Sci. Instrum.* **2001**, *72*, 2855.
32 T. Ichimura, N. Hayazawa, M. Hashimoto, Y. Inouye, S. Kawata, *Phys. Rev. Lett.* **2004**, *92*, 220801.
33 R. D. Schaller, J. Ziegelbauer, L. F. Lee, L. H. Haber, R. J. Saykally, *J. Phys. Chem. B* **2002**, *106*, 8489.
34 C. Heinrich, S. Bernet, M. Ritsch-Marte, *Appl. Phys. Lett.* **2004**, *84*, 816.
35 X. Nan, E. O. Potma, X. S. Xie, *Biophys. J.* **2006**, *91*, 728.
36 Y. Fu, H. Wang, T. B. Huff, R. Shi, J.-X. Cheng, *J. Neurosci. Res.* **2007**, *85*, 2870.
37 L. Tong, Y. Lu, R. J. Lee, J.-X. Cheng, *J. Phys. Chem. B* **2007**, *111*, 9980.
38 E. Kang, H. Wang, I. K. Kwon, J. Robinson, K. Park, J.-X. Cheng, *Anal. Chem.* **2006**, *78*, 8036.
39 X. Nan, A. M. Tonary, A. Stolow, X. S. Xie, J. P. Pezacki, *ChemBioChem* **2006**, *7*, 1895.
40 S. O. Konorov, C. H. Glover, J. M. Piret, J. Bryan, H. G. Schulze, M. W. Blades, R. F. B. Turner, *Anal. Chem.* **2007**, *79*, 7221.
41 T. Hellerer, C. Axäng, C. Brackmann, P. Hillertz, M. Pilon, A. Enejder, *Proc. Natl. Acad. Sci. U.S.A.* **2007**, *104*, 14658.
42 C. L. Evans, X. Xu, S. Kesari, X. S. Xie, S. T. C. Wong, G. S. Young, *Opt. Express* **2007**, *15*, 12076.
43 H.-W. Wang, N. Bao, T. L. Le, C. Lu, J.-X. Cheng, *Opt. Express* **2008**, *16*, 5782.
44 M. H. F. Kox, K. F. Domke, J. P. R. Day, G. Rago, E. Stavitski, M. Bonn, B. M. Weckhuysen, *Angew. Chem., Int. Ed.* **2009**, *48*, 8990.
45 C. W. Freudiger, W. Min, B. G. Saar, S. Lu, G. R. Holtom, C. He, J. C. Tsai, J. X. Kang, X. S. Xie, *Science* **2008**, *322*, 1857.
46 H. Kano, H. Hamaguchi, *Anal. Chem.* **2007**, *79*, 8967.
47 C. Otto, A. Voroshilov, S. G. Kruglik, J. Greve, *J. Raman Spectrosc.* **2001**, *32*, 495.
48 J.-X. Cheng, A. Volkmer, L. D. Book, X. S. Xie, *J. Phys. Chem. B* **2002**, *106*, 8493.
49 G. W. H. Wurpel, J. M. Schins, M. Müller, *Opt. Lett.* **2002**, *27*, 1093.
50 D. Oron, N. Dudovich, Y. Silberberg, *Phys. Rev. Lett.* **2003**, *90*, 213902.
51 J. K. Ranka, R. S. Windeler, A. J. Stentz, *Opt. Lett.* **2000**, *25*, 25.
52 P. Russell, *Science* **2003**, *299*, 358.
53 P. St. J. Russell, *J. Lightwave Technol.* **2006**, *24*, 4729.
54 J. M. Dudley, G. Genty, S. Coen, *Rev. Mod. Phys.* **2006**, *78*, 1135.
55 F. G. Omenetto, N. A. Wolchover, M. R. Wehner, M. Ross, A. Efimov, A. J. Taylor, V. V. R. K. Kumar, A. K. George, J. C. Knight, N. Y. Joly, P. St. J. Russell, *Opt. Express* **2006**, *14*, 4928.
56 P. Domachuk, N. A. Wolchover, M. Cronin-Golomb, A. Wang, A. K. George, C. M. B. Cordeiro, J. C. Knight, F. G.

Omenetto, *Opt. Express* **2008**, *16*, 7161.
57 P.-A. Champert, V. Couderc, P. Leproux, S. Février, V. Tombelaine, L. Labonté, P. Roy, C. Froehly, P. Nérin, *Opt. Express* **2004**, *12*, 4366.
58 V. Tombelaine, C. Lesvigne, P. Leproux, L. Grossard, V. Couderc, J.-L. Auguste, J.-M. Blondy, G. Huss, P.-H. Pioger, *Opt. Express* **2005**, *13*, 7399.
59 K. Shi, P. Li, S. Yin, Z. Liu, *Opt. Express* **2004**, *12*, 2096.
60 G. McConnell, E. Riis, *J. Biomed. Opt.* **2004**, *9*, 922.
61 G. McConnell, *Opt. Express* **2004**, *12*, 2844.
62 K. Lindfors, T. Kalkbrenner, P. Stoller, V. Sandoghdar, *Phys. Rev. Lett.* **2004**, *93*, 037401/1.
63 K. Isobe, W. Watanabe, S. Matsunaga, T. Higashi, K. Fukui, K. Itoh, *Jpn. J. Appl. Phys.* **2005**, *44*, L167.
64 J. Palero, V. Boer, J. Vijverberg, H. C. Gerritsen, H. J. C. M. Sterenborg, *Opt. Express* **2005**, *13*, 5363.
65 C. Dunsby, P. M. P. Lanigan, J. McGinty, D. S. Elson, J. Requejo-Isidro, I. Munro, N. Galletly, F. McCann, B. Treanor, B. Önfelt, D. M. Davis, M. A. A. Neil, P. M. W. French, *J. Phys. D: Appl. Phys.* **2004**, *37*, 3296.
66 D. M. Grant, D. S. Elson, D. Schimpf, C. Dunsby, J. Requejo-Isidro, E. Auksorius, I. Munro, M. A. Neil, P. M. French, E. Nye, G. Stamp, P. Courtney, *Opt. Lett.* **2005**, *30*, 3353.
67 H. N. Paulsen, K. M. Hilligse, J. Thøgersen, S. R. Keiding, J. J. Larsen, *Opt. Lett.* **2003**, *28*, 1123.
68 T. W. Kee, M. T. Cicerone, *Opt. Lett.* **2004**, *29*, 2701.
69 H. Kano, H. Hamaguchi, *Opt. Express* **2005**, *13*, 1322.
70 B. von Vacano, W. Wohlleben, M. Motzkus, *Opt. Lett.* **2006**, *31*, 413.
71 H. Kano, H. Hamaguchi, *Opt. Express* **2006**, *14*, 2798.
72 D. Wildanger, E. Rittweger, L. Kastrup, S. W. Hell, *Opt. Express* **2008**, *16*, 9614.
73 P. Li, K. Shi, Z. Liu, *Opt. Lett.* **2005**, *30*, 156.
74 B. von Vacano, T. Buckup, M. Motzkus, *Opt. Lett.* **2006**, *31*, 1154.
75 H. Kano, R. Shimada, H. Hamaguchi, *Oyo Butsuri* **2006**, *75*, 682.
76 H. Kano, *Mol. Sci.* **2007**, *1*, A0005.
77 H. Kano, H. Hamaguchi, *J. Phys. Chem. B* **2006**, *110*, 3120.
78 G. W. H. Wurpel, J. M. Schins, M. Müller, *J. Phys. Chem. B* **2004**, *108*, 3400.
79 E. M. Vartiainen, H. A. Rinia, M. Müller, M. Bonn, *Opt. Express* **2006**, *14*, 3622.
80 H. Kano, H. Hamaguchi, *Chem. Lett.* **2006**, *35*, 1124.
81 N. P. Ivleva, R. Niessner, U. Panne, *Anal. Bioanal. Chem.* **2005**, *381*, 261.
82 A. Sengupta, M. L. Laucks, E. J. Davis, *Appl. Spectrosc.* **2005**, *59*, 1016.
83 G. W. H. Wurpel, M. Müller, *Chem. Phys. Lett.* **2006**, *425*, 336.
84 R. M. Onorato, N. Muraki, K. P. Knutsen, R. J. Saykally, *Opt. Lett.* **2007**, *32*, 2858.
85 G. I. Petrov, R. Arora, V. V. Yakovlev, X. Wang, A. V. Sokolov, M. O. Scully, *Proc. Natl. Acad. Sci. U.S.A.* **2007**, *104*, 7776.
86 M. Okuno, H. Kano, P. Leproux, V. Couderc, H. Hamaguchi, *Opt. Lett.* **2007**, *32*, 3050.
87 M. Okuno, H. Kano, P. Leproux, V. Couderc, H. Hamaguchi, *Opt. Lett.* **2008**, *33*, 923.
88 R. Shimada, H. Kano, H. Hamaguchi, *Opt. Lett.* **2006**, *31*, 320.

Hideaki Kano is currently Associate Professor of the Graduate School of Science, the University of Tokyo. He was born in Tokushima, Japan, in 1974. He graduated from the Department of Physics, School of Science, the University of Tokyo in 1996. He received his M.Sc. and D.Sc. from the University of Tokyo in 1998 and 2001, respectively. He was appointed as Research Associate at the University of Tokyo in 2001, and promoted to the present position in 2007. Since 2007, he has been a PRESTO researcher of the Japan Science and Technology Agency (JST). His research interests involve developing spectroscopic methods using novel nonlinear optical processes for imaging biological molecules in living cells and living organisms at the molecular level.